Structured-illumination Makyoh-topography: Optimum grid position and its constraints

Ferenc Riesz

Hungarian Academy of Sciences, Centre for Energy Research, Institute for Technical Physics and Materials Science, P.O. Box 49, H–1525 Budapest, Hungary

E-mail: riesz.ferenc@energia.mta.hu

Abstract

Complementing conventional Makyoh topography with structured illumination using a sparse square grid, the large-scale surface shape can be calculated with a deflectometry approach, while the sample's morphology can still be imaged. However, the grid's image must be sharp not to mask the Makyoh image of the sample morphology. In this paper, the instrumental conditions for the grid sharpness are established. The two main types of Makyoh set-ups (lens and mirror based) are analysed. It is shown that the lens-based set-ups allow the position of the grid to be sharp on the Makyoh image. However, for mirror-based set-ups this is not possible because of geometrical instrumental constraints. The calculations are corroborated with experiments.

Keywords: flatness testing, surface defects, Makyoh topography, structured illumination, deflectometry, geometrical optics

Published in: Surf. Topogr.: Metrol. Prop. 6 (2018) 045009.
https://doi.org/10.1088/2051-672X/aaeb86

Introduction and basic concepts

Makyoh (or magic-mirror) topography is a powerful optical tool for the qualitative assessment of the surface quality of closely flat, mirror-like surfaces [1-4]. The word Makyoh means 'magic mirror' in Japanese; it refers to an ancient mirror of sacred use that projects an image to a distant wall when the mirror is shone by the sun. The image is formed due to small flatness deviations of the reflecting surface: these irregularities act as convex or concave mirror regions that focus or defocus the reflected beam. Makyoh topography is based on a similar principle: the surface under test is illuminated by a uniform-intensity collimated light beam, and a reflected image is formed on a screen placed some distance away from the sample. The sample surface morphology is thus revealed as dark/bright contrast patches in the image, corresponding to convex/concave surface regions. In spite of the progress in the understanding of the Makyoh imaging formation mechanism [5, 6], the method remained chiefly qualitative in practice as a kind of visual tool. The method's advantages, as compared to concurrent optical methods such as interferometry and deflectometry, are the extreme simplicity, low cost, no need for accurate sample positioning and calibration, real-time operation and high dynamic range [1, 4]. Makyoh topography found its most fruitful applications in semiconductor technology (both in laboratory and production environment) for in-line detection of surface defects [1-3], where qualitative detection is sufficient, and instant operation is required.

Within the geometrical optical approximation [5], Makyoh imaging can be treated as a mapping of the surface plane onto the image plane according to the gradient field of the surface, whereas the intensity of the image points are determined by the local curvatures of the corresponding surface points. This gradient-related mapping means a kind of image distortion [7]. The key parameter of the imaging is the screen-to-surface distance. Increasing this distance increases the image contrast, thus, sensitivity, but also the amount of the image distortion. See references [5, 7] for further details of the model.

After some initial work [8], it has been shown that applying structured illumination, a useful quantitative version of Makyoh topography can be realised [9]. That is, by inserting a periodic mask (e.g., a square grid) in the path of the illuminating beam, the surface shape can be determined at the grid nodes by integrating the gradients obtained through the displacement of the grid node positions in the image as compared to those pertaining to a flat surface. For high lateral resolution and avoiding aliasing effects, a dense grid is desirable. A dense grid, however, masks the original Makyoh image, thus hindering the observation of the morphology: the method can no longer be strictly treated as 'Makyoh topography', rather, we obtain a variation of the well known deflectometry [10] methods. (We note here that in this 'deflectomery mode', the mask does not need to be a grid; any two-dimensional periodic pattern, e.g., a Hartmann mask is suitable.) We have explored this method earlier: the grid nodes in the image were localised using a two-step correlation procedure [11] and the two-dimensional integration of the gradient field was implemented [9] as a line integration or an iterative process. The details of the evaluation algorithm as well as the application of the method in semiconductor technology have been presented in our previous papers [4, 9, 12, 13].

The limitation discussed above (that is, losing the high-resolution morphology-related contrast due to the masking by the grid) can however be circumvented using a suitable mask (grid) geometry and instrumental arrangement. That is, if the grid is sufficiently sparse, the lines are thin and its image is closely sharp in the Makyoh image, the sample

morphology can still be observed qualitatively with high spatial resolution as in conventional Makyoh topography, so as blurring or excessive diffraction effects of the mask pattern do not cover large image areas. Simultaneously, the grid constitutes a basis for the quantitative measurement of the sample height map at low spatial resolution with the deflectometry approach detailed above. In addition, the grid contains easily accessible visual information on the large-scale surface shape as well: denser grid regions in the image indicates concave sample regions (for positive screen-to-sample distance). Also, as the grid nodes represent real sample positions, the image distortion [7] can be visualised and the image points can be assigned to the corresponding sample points. Thus the grid also aids in the qualitative Makyoh observation. We note finally that using the grid pattern as a mask is essential, as (unlike, e.g., the Hartmann mask) it is mostly transparent, further, it is well observable even in a 'busy' image; in addition, it ensures safe localisation of the node positions using a correlation procedure even for highly structured sample morphologies [11]. To recapitulate: we obtain a 'two-channel' tool, where the conventional qualitative Makyoh topography is retained, while the large-scale sample height map can be measured using the deflectometry methodology.

Since the deflectometry part has been presented in our earlier publications (see above), in the present paper we deal with the grid sharpness issue only. The paper is organised as follows. First, we describe the Makyoh-topography set-ups used in practice. Next, we formulate quantitative conditions for the grid sharpness, then, the instrumental requirements for the sharpness are analysed. The two common types of Makyoh set-ups (lens and mirror based) are compared. The model is corroborated with experiments.

Makyoh-topography set-ups

Since a Makyoh topogram is essentially a defocussed reflected image of the sample, the most basic form of Makyoh-topography set-ups consists only of a light source providing a collimated beam and a distant screen [6]. The screen-to-sample distance can be changed by moving the screen along the optical axis. However, practical (laboratory or industrial) applications should allow the use of electronic cameras, should have a compact size and the imaging parameters should be changed conveniently. A widely used set-up [1, 4] meets these requirements as follows. This arrangement incorporates a converging lens positioned close to the sample. This lens has a double role: (1) it collimates the light beam of the point source placed in the focus of the lens, providing the illuminating beam and (2) converges the nearly parallel reflected beam to the camera, since the camera's aperture is usually much smaller than the sample size. The lens thus serves as a kind of 'magnifier' in addition to the collimator role. In order to intercept the whole cross section of the reflected beam, the camera's lens has to be placed close to the focal plane of the magnifier. Adjusting the camera lens' object distance is an easy way of varying the equivalent screen-to-sample distance. In this set-up, the lens' diameter limits the maximum surface area that can be studied. Using concave (spherical or parabolic) mirror(s) instead of the lens enables larger measurement aperture since mirrors can be manufactured in larger diameters (also, internal reflections and chromatic aberrations are avoided). However, the sample has to be placed farther away from the mirrors to allow enough space for the illuminating and reflected beams [14]. Figure 1 shows schematically the set-ups discussed above. These set-ups have been analysed in terms of the equivalent screen-to-sample distance and magnification in reference [15].

Slightly different, but optically equivalent set-ups are also in use that include beam splitters as well [14, 16].

Analysis

The rigorous optical modelling of the grid's image would involve the calculation of the diffraction of an arbitrary grid geometry (line thickness and pitch), for arbitrary sample surface figure, taking into account also the spatial and spectral properties of the light source. This is a formidable task well beyond the scope of the paper. For our analysis we resort to a simple model with ideal point source, monochromatic illumination, flat sample, and simplified grid geometry. In this approximation, the measure of the sharpness of the grid's image for a given grid geometry can be described solely by the distance L_c between the grid and the conjugate plane of the camera sensor as imaged by the whole optical system, and the distance between the grid and the light source. For a sharp grid image, $L_c = 0$. L_c is thus an instrumental parameter depending on the position and optical properties (focal length) of the optical elements and the grid only. The acceptable values of L_c are therefore determined by the grid geometry and the tolerable amount of the grid masking in the observed image. In the following, we give a rough estimate of the maximum allowable L_c values, then analyse its dependence on the instrumental parameters.

In general, the diffraction pattern of a grid is described by the Talbot effect [17]. The Talbot effect is characterised by the Talbot length $z_T = 2a^2/\lambda$ (for $a >> \lambda$, and plane-wave incidence), the distance where the grid image repeats itself; here a is the grid pitch and λ is the wavelength. For visible light and a in the order of a few millimetres, z_T is in the order of 10 m. However, as Talbot patterns appear when the individual diffraction patterns of the grid lines start to overlap, a more strict condition is imposed by the diffraction of the individual grid lines. The full formulae describing this diffraction effect are rather complex, even if the grid lines are modelled as infinitely long opaque strips [18]; however the phenomenon is chiefly governed by the Fresnel diffraction at an edge [19]. Infinite source distance is assumed, thus the magnification caused by the divergent illumination is removed from the result; this simplification is justified only if L_c is much smaller than the grid-source distance [19]. However, at larger L_c, the validity of the half-plane Fresnel approximation is questionable. The intensity peak of the first fringe in Fresnel diffraction situates at the distance of roughly $w = (\lambda L_c)^{1/2}$ from the geometrical shadow edge. The extension of the well visible fringes is about a few times this value. In the ideal case, the modulation value characterising the fringe contrast (between first maximum and first minimum) around the distance w from the shadow edge is about 30%, while at $2w$, it is about 17%. However, in a practical setting, the fringe visibility is deteriorated by the finite source size and limited coherency. The optimum modulation values in Makyoh for safe contrast discrimination are typically greater than 10% [7]. Therefore, as a rough guide, $2w$ can be taken as a masking width of the fringes. A practically useful limit of the acceptable diffraction can thus be set by equating this distance to a definite fraction of the grid pitch. Taking this ratio (somewhat arbitrarily) as 10%, we obtain $L_c < a^2/(0.2\ \mathrm{mm})$ at visible wavelengths ($\lambda = 0.5\ \mu\mathrm{m}$). We recapitulate that this must be considered as a very soft and approximate limit.

Next, we determine the position of the grid's image as seen by the camera lens in order to assess the conditions for its sharpness in the Makyoh image. The lens and mirror-based systems can be treated in a unified way as follows. For clarity, consider a 'folded-out', transmission-like model representation of the set-ups (figure 2). Figure 2 also introduces our

notation: the grid-to-collimator distance is g, the sample-to-lens (or mirrors) distance is D, and the focal length of the lens (or mirrors) is f. The collimator lens images the grid to the virtual position 1 (distance from the collimator, g_1), then, this image is further imaged by the magnifier lens to the virtual position 2 (distance from the magnifier, g_2). This latter is the position as seen by the camera lens. L_c thus can be found as the distance between position 2 and the camera's set object distance. The value of g_2 can be simply calculated by the successive application of the lens formula. (Note that we assume the sample to be perfectly flat, which is not true in the practice; however, the curvature radii characterising the sample deformation are usually much larger than the focal lengths, so it has a negligible effect on the sharpness.) It is purposeful to normalise the distances by f. Omitting the straightforward calculation, we obtain:

$$g_2 = \frac{2D^*(g^*-1)-g^*}{(2D^*-1)(g^*-1)-g^*}, \qquad (1)$$

where the asterix denotes normalised values. Figure 3 shows the graph of this formula, parametrised by D^*. This graph tells us that changing either D or g has a dramatic effect on g_2. However, the practical instrumental limit for g^* is roughly in the 0.4 to 0.9 range to avoid the shadowing of the reflected beam by the grid.

Now we further investigate two limiting special cases. These are just the characteristic cases corresponding to the two set-ups we are dealing with. At $D = 0$, we get the approximate case of the lens-based set-up, where the lens is placed close to the sample, while, at $D = f$ we obtain a characteristic and purposeful realisation of the mirror-based system [14]. Rewriting formula (1) for these cases we obtain:

$$g_2^*(D = 0) = \frac{g^*}{2g^*-1}, \qquad (2)$$

and

$$g_2^*(D = f) = 2 - g^*. \qquad (3)$$

Since the camera lens-magnifier lens distance, c roughly equals f, for $g_2^* > 1$, the sharpness condition is never fulfilled (the grid's image is behind the camera lens) in the mirror-based systems. As L_c is the sum of g_2 and the camera lens object distance setting it is typically in the range of a few metres, which results in an unacceptable high amount of diffraction. We note also that the dependence of the grid virtual position on the grid position is weak. Summarising, the mirror-based systems are not suitable for the simultaneous operation in deflectometry and conventional Makyoh mode. (Of course, they can still be used either for qualitative studies with no grid or in deflectometry mode with grid but not in the "two-channel" mode.)

In contrast, for the lens-based systems, it is easy to ensure the grid sharpness: by positioning the grid in the $g^* < 0.5$ range, sharpness can be reached for a wide range of camera lens object distance settings, since the grid virtual image will be far in the left side in figure 2. At $g^* = 0.5$, the grid image is at infinity; at infinity camera lens setting, the grid will be sharp.

To complete the picture, we give the dependence of the equivalent screen-to-sample distance, L on the instrumental parameters (for a detailed analysis, see reference [15]). The general formula is:

$$L = D - \frac{1}{1/f + 1/(k-c)}. \quad (4)$$

Here k is the object distance set on the camera lens. Again, approximating D = 0, and considering that for usual L settings k >> c, we obtain:

$$L_{lens} = -\frac{1}{1/f + 1/k}. \quad (5)$$

For the mirror based systems, we can approximate $D = f$ and similarly, $c = f$, thus (4) reduces to:

$$L_{mirror} = f^2/k. \quad (6)$$

Experimental results

Our experiments' purpose is to demonstrate the calculations presented above. The lens-based set-up [4] we used applies a 500-mm focal-length converging lens as a collimator/magnifier, and an 820-nm pigtailed LED as a point source. The camera lens-magnifier distance is about 470 mm. The mirror-based set-up [14] uses two 914.4-mm focal-length spherical mirrors. A yellow chip LED (specified wavelength, 592 nm) serves as a point source. The camera lens was placed approximately at the focal plane of the magnifier mirror. The camera in both set-ups is a 1280 × 960 pixel resolution b/w camera with a 2/3″ CCD sensor equipped with a 75-mm focal length objective. The grid (applied in both set-ups) was formed by photolitography on a flat glass substrate with a = 2 mm pitch and 200-µm line width. These correspond to a limit to L_c as 23.5 mm and 17 mm for the lens and mirror based system, respectively. As a test sample, we used a 2-inch Si wafer having a backside scratch, some global deformation and other localised morphological features.

For the lens-based set-up, the value L was set to -400 mm (for lens based systems, L is chiefly negative, see (5)), corresponding to the camera lens distance setting of 4 m. This L value was chosen to observe a good-contrast Makyoh image. Figure 4 shows the gridless Makyoh image of the sample. For negative L, the dark (bright) image areas indicate concave (convex) sample areas. The vertical dark band in the middle area is a characteristic signature of the backside scratch which creates a concave sample deformation [20]. The topogram also shows the images of other surface defects and features: (1) line-like features at the wafer periphery parallel to the main crystallographic axes; these are images of dislocation slip line bunches as confirmed by the comparison of Makyoh and x-ray topography in other experiments [21], (2) localised, circular-shaped defects in the lower left quarter of the wafer, (3) a slowly varying contrast due to global deformation and (4) an overall speckle [22] indicating surface roughness. Figures 5 and 6 show the Makyoh images at the same L setting but with a grid. In figure 5, the grid was positioned to obtain its sharp image: at this setting, g was 290 mm (in agreement with (1)); the morphological features detailed above are clearly visible, they are not masked by the grid's image. In contrast, in figure 6, g is set to 390 mm to demonstrate the masking effect of the diffraction features. Indeed, in this topogram, the speckle contrast and the images of the localised defects are hardly visible, and the fine structure of the scratch image and the slip lines is masked, however the slowly varying intensity is still visible. Note also that the diffraction fringes have high contrast, higher than most defect-related Makyoh contrast.

For the mirror-based set-up, L was set to 400 mm to observe a similar character of the Makyoh contrast to that of the lens-based set-up (for mirror based systems, L is always positive, see equation (6)). At this

setting, the object distance set on the camera lens was 2 m. Figure 7 shows the Makyoh image without the grid. The image shows the same morphological features as in the lens-based case, however the opposite-sign L renders the contrast the opposite. For example, the scratch's image is now a bright band [20]. In figure 8, the grid was positioned at g = 600 mm. Moving the grid, the diffraction width changes slowly, as predicted by equation (1). Fractional Talbot patterns are also clearly observed. The diffraction patterns completely mask the fine morphological features: the speckle contrast and the localised defects are invisible, only the scratch-related centre feature and some high-contrast slip-line images are observable but the details are smeared. However, the diffraction-related contrast is weak, which has a beneficial effect of allowing the high-contrast Makyoh image features somehow visible.

Conclusions

Structured illumination using a grid is a fruitful concept in Makyoh topography, as it allows computing the large-scale surface shape, and aids in qualitative visual evaluation as well. Lens-based set-ups allow to position the grid to be sharp on the Makyoh image, facilitating the simultaneous observation of the sample morphology. However, for mirror-based set-ups this is not possible because of geometrical instrumental constraints.

Acknowledgements

The author is grateful to Makai J P for experimental contributions. This work was supported, in part, by the National Research, Development and Innovation Fund of the Hungarian Government (KoFAH, NVKP_16-1-2016-0018).

ORCID iD

http://orcid.org/0000-0003-4334-8544

References

[1] Blaustein P and Hahn S 1989 Realtime inspection of wafer surfaces *Solid State Technol.* 32 27-9

[2] Hahn S, Kugimiya K, Vojtechovsky K, Sifalda M, Yamashita M, Blaustein PR and Takahashi K 1992 Characterisation of mirror-polished Si wafers and advanced Si substrate structures using the magic mirror method *Semicond. Sci. Technol.* 7 A80–5

[3] Young H T, Liao H-T and Huang H-Y 2006 Surface integrity of silicon wafers in ultra precision machining *Int. J. Adv. Manuf. Technol.* 29 372–8

[4] Riesz F 2004 Makyoh topography: a simple yet powerful optical method for flatness and defect characterisation of mirror-like surfaces *Proc. SPIE* 5458 86–100

[5] Riesz F 2000 Geometrical optical model of the image formation in Makyoh (magic-mirror) topography *J. Phys. D: Appl. Phys.* 33 3033–40

[6] Laczik Z J 2000 Quantitative Makyoh topography *Opt. Eng.* 39 2562–7

[7] Riesz F 2013 Non-linearity and related features of Makyoh (magic-mirror) imaging *J. Optics* 15 075709

[8] Yang K H 1985 An optical imaging method for wafer warpage measurements *J. Electrochem. Soc.* 132 1214–8

[9] Lukács I E and Riesz F 2004 Error analysis of Makyoh-topography surface height profile measurements *Eur. Phys. J. – Appl. Phys.* 27 385–8

[10] Muñoz-Potosi A F, Granados-Agustín F, Campos-García M, Valdivieso-González L G and Percino-Zacarias M E 2017 Deflectometry using a Hartmann screen to measure tilt, decentering and focus errors in a spherical surface *Opt. Comm.* 402 375-81

[11] Lukács I E and Riesz F 2008 Sub-pixel detection of a grid's node positions for optical diagnostics *Thin Solid Films* 516 8082-6

[12] Lukács I E, Vízváry Zs, Fürjes P, Riesz F, Dücsö Cs and Bársony I 2002 Determination of deformation induced by thin film residual stress in structures of millimetre size *Adv. Eng. Mater.* 4 625-7

[13] Lukács I E and Riesz F 2003 Makyoh-topography assessment of etch and polish removal of processed circuits for substrate re-use *Microel. Eng.* 65 380-6

[14] Makai J P, Riesz F and Lukács I E 2006 Practical realizations of the Makyoh (magic mirror) arrangement for the investigation of large area mirror-like surfaces *Proc. 3rd Int. Conf. on Metrology, Trends and Applications in Calibration and Testing Laboratories, Tel Aviv, Nov 14-16*

[15] Riesz F 2001 Camera length and field of view in Makyoh-topography instruments *Rev. Sci. Instr.* 72 1591–3

[16] Jiajun Tian, Yong Yao, Yunxu Sun, Weijie Shi, Xinhui Zhao and Xuelian Yu 2007 Research of light reflex surface defects detection technology *Proc. SPIE* 6834 683418

[17] Berry M V and Klein 1996 Integer, fractional and fractal Talbot effect *J. Mod. Opt.* 43 2139-64

[18] Šmíd P and Horváth P 2012 Fresnel diffraction at an opaque strip expressed by means of asymptotic representations of Fresnel integrals *J. Opt. Soc. Am. A* 29 1071-7

[19] Jenkins F A and White H E 1981 *Fundamentals of Optics, 4th ed.* (Singapore: McGraw-Hill) p. 393

[20] Riesz F 2000 Makyoh-topography study of grooves scratched and etched in single-crystal semiconductors *Mater. Letters* 46 291-5

[21] Kugimiya K 1992 Makyoh topography: comparison with X-ray topography *Semicond. Sci. Technol.* 7 A91-4

[22] Riesz F 2011 Effects of speckle in Makyoh topography for the studies of extended defects *J. Phys. Conf. Ser.* 281 012006

Figure captions

Figure 1. Makyoh-topography set-ups: (a) using collimated illumination and screen, (b) lens-based and (c) mirror-based set-ups.

Figure 2. Schematic representation of the grid in Makyoh set-ups.

Figure 3. Calculated position of the virtual grid image as a function of the grid position, parametrised with D^*.

Figure 4. Makyoh-topography image of the sample taken with the lens-based set-up at L = -400 mm, without the grid.

Figure 5. Makyoh-topography image of the sample taken with the lens-based set-up at L = -400 mm, with grid position at g = 280 mm.

Figure 6. Makyoh-topography image of the sample taken with the lens-based set-up at L = -400 mm, with grid position at g = 390 mm.

Figure 7. Makyoh-topography image of the sample taken with the mirror-based set-up at L = 400 mm, without the grid.

Figure 8. Makyoh-topography image of the sample taken with the mirror-based set-up at L = 400 mm, with grid position at g = 600 mm.

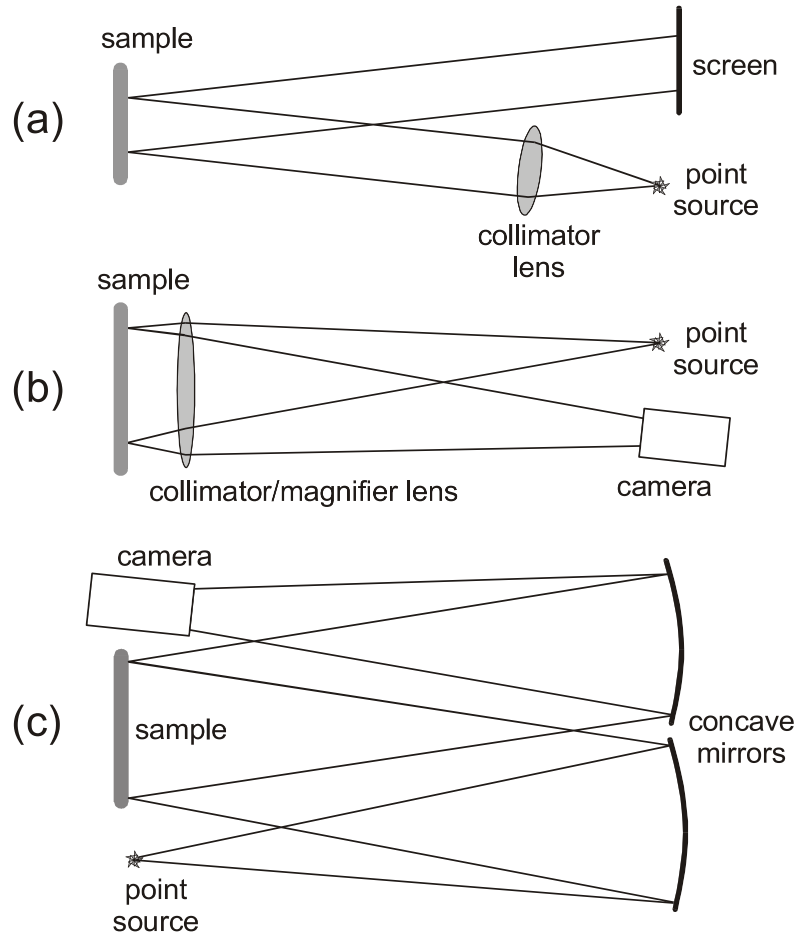

Figure 1

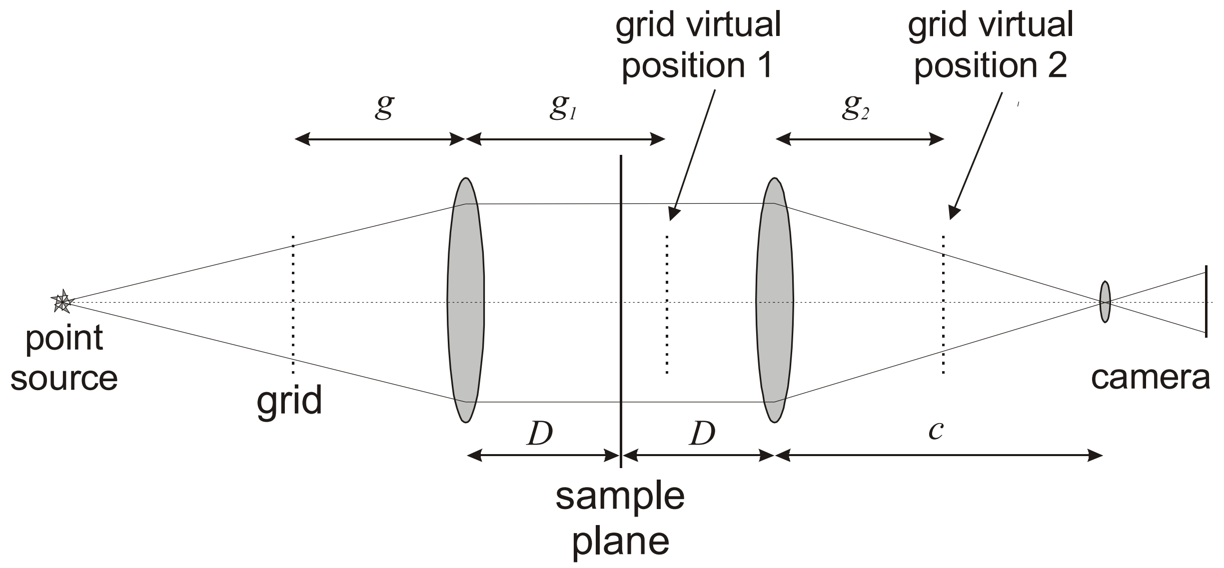

Figure 2

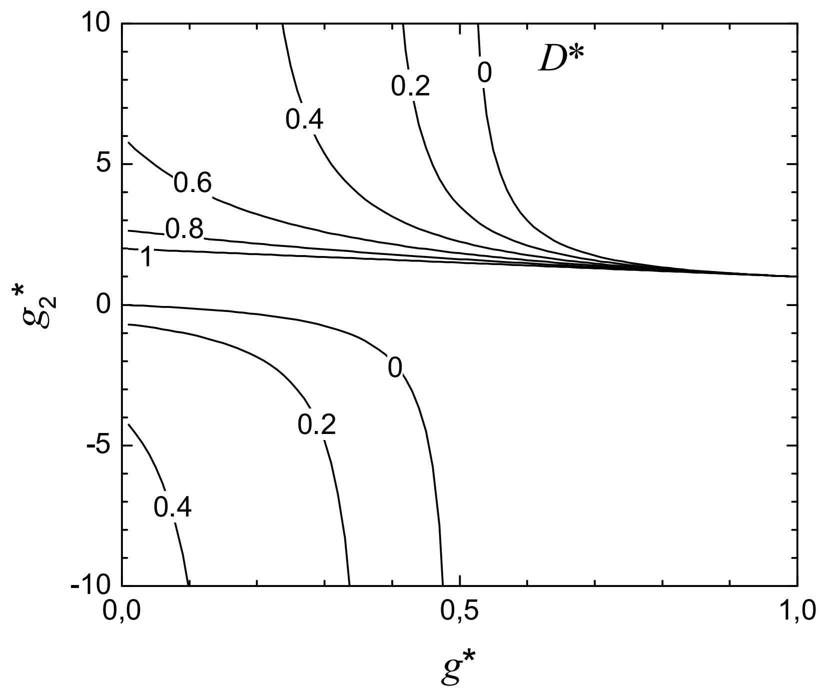

Figure 3

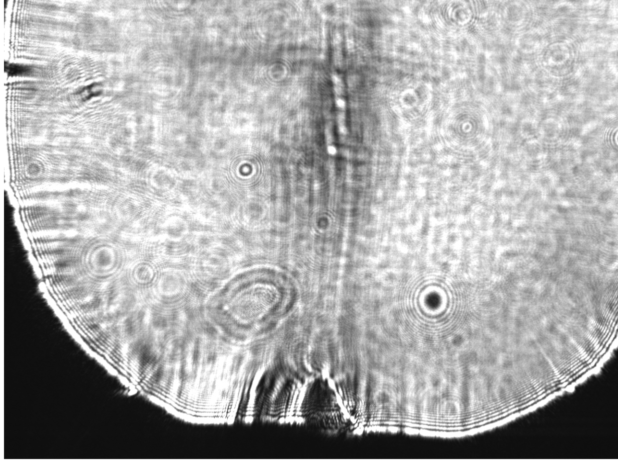

Figure 4

Figure 5

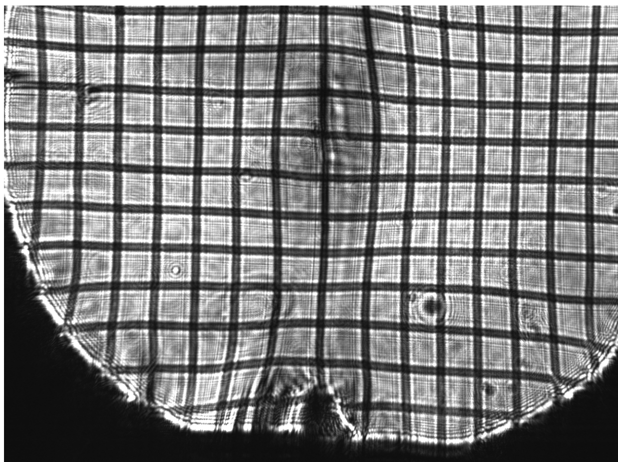

Figure 6

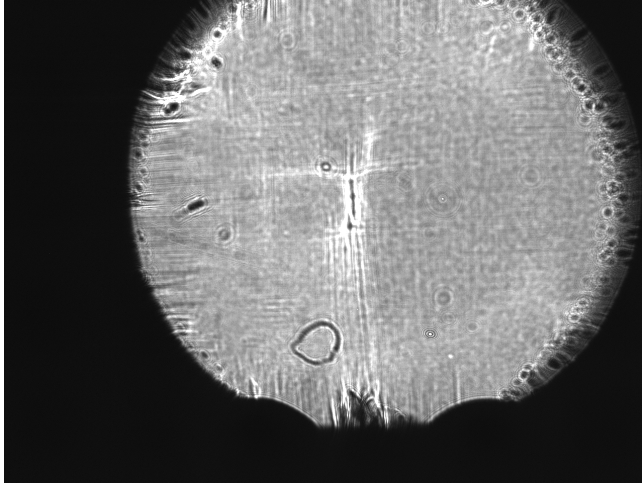

Figure 7

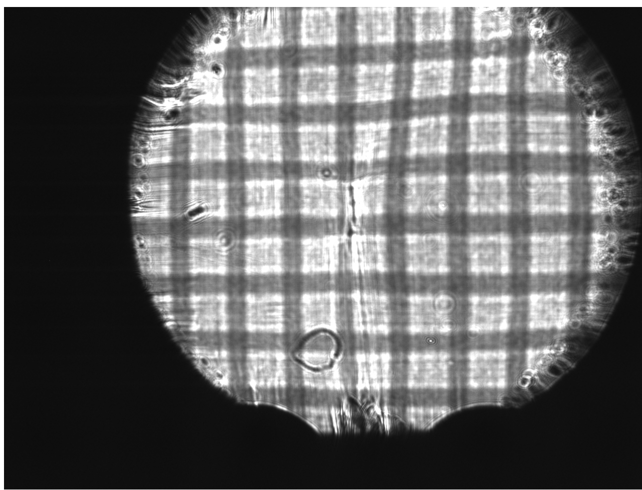

Figure 8